Structural, AC conductivity, dielectric behavior and magnetic properties of Mg–substituted LiFe5O8 powders synthesized by...

Article *in* Journal of Materials Science Materials in Electronics · May 2015

DOI: 10.1007/s10854-015-3181-2

CITATION
1

READS
69

5 authors, including:

M. G. El-Shaarawy
Benha University
36 PUBLICATIONS **277** CITATIONS
SEE PROFILE

Mohamed M Rashad
Central Metallurgical Research and Develop...
149 PUBLICATIONS **1,990** CITATIONS
SEE PROFILE

N. M. Shash
Benha University
32 PUBLICATIONS **108** CITATIONS
SEE PROFILE

J Mater Sci: Mater Electron (2015) 26:6040–6050
DOI 10.1007/s10854-015-3181-2

Structural, AC conductivity, dielectric behavior and magnetic properties of Mg-substituted $LiFe_5O_8$ powders synthesized by sol–gel auto-combustion method

M. G. El-Shaarawy[1] · M. M. Rashad[2] · N. M. Shash[1] · M. H. Maklad[1] · F. A. Afifi[3]

Received: 7 April 2015 / Accepted: 8 May 2015 / Published online: 14 May 2015

Abstract Magnesium-substituted lithium ferrite powders ($Li_{1-x}Mg_{2x}Fe_{5-x}O_8$ where x = 0.0–0.8) were prepared by sol–gel auto-combustion method. XRD profiles revealed that all compositions were single cubic ferrite structure for the precursors annealed at 800 °C for 2 h. The crystallite size was found to decrease whereas the lattice parameter was increased with increasing Mg^{2+} ion content. The microstructure of the formed powders was Mg concentration dependent. Increasing the Mg^{2+} ion ratio was found to inhibit the grain growth of the formed ferrite. The AC electrical conductivity of Mg^{2+} ion substituted lithium ferrite samples was raised with increasing the concentration of Mg^{2+} ions as the result of increasing the hopping of electrons between Fe^{2+} and Fe^{3+} ions. Meanwhile, dielectric constant (ε′) was diminished with increasing the frequency of external electric field as well as increasing the temperature and concentration of Mg^{2+} ions. Alongside, the formed crystalline magnesium substituted lithium ferrite had good magnetic properties. High saturation magnetization (78.7 emu/g) was attained by the formed ferrite sample at Mg^{2+} molar ratio of 0.4 annealed at 800 °C for 2 h.

✉ M. M. Rashad
rashad133@yahoo.com

[1] Physics Department, Faculty of Science, Benha University, Benha, Egypt

[2] Central Metallurgical Research and Development Institute (CMRDI), Helwan, Cairo, Egypt

[3] Basic Engineering Science Department, Faculty of Engineering, Benha University, Benha, Egypt

1 Introduction

Recent developments of lithium ferrite have attracted a lot of research interest due to advantageous properties such as high saturation magnetization, low dielectric losses and excellent square shaped of hysteresis curve, excellent dielectric properties, high resistivity $\sim 10^8$ Ω cm, lower eddy current, relatively high Curie temperature (620 °C), high chemical inertness, thermal stability, high resistivity and low eddy current losses, low cost and safety. Due to these unique properties, it promises to be a potential prolonged application for microwave devices instead of expensive yttrium iron garnet (YIG) like circulators, phase shifters, isolators, power transformation in electronics, memory core, antennas and high-speed digital tapes. Furthermore, it is exploited for lithium ion batteries, high-density magnetic recording, magnetic fluids, magneto-caloric refrigeration, magnetic resonance imaging enhancement, magnetically guided drug delivery and multilayer chips inductors [1–5]. The properties of lithium ferrite can be tailored by controlling the synthesis process and the suitable substitution of metal ions. Numerous wet chemical methods have been applied to synthesize lithium ferrite fine particles including ball milling [4], sol–gel [6], combustion method [7, 8], hydrothermal [5, 10, 11], solvothermal [12], aerosol route [13] co-precipitation [14] and microemulsion [14] techniques. It is claim mentioning that ferrites powders prepared by sol–gel auto-combustion method technique at low annealing temperature possesses homogeneous microstructure, fine particle size, narrow size distribution, minimum particle agglomeration good chemical purity and improved physical properties [15–18]. Meanwhile, the origin of magnetic and dielectric properties of lithium ferrite is regarded to the variety of metal substitution. The effect of Mn [2], Zn [2], Co [9, 19], Ce [20], Cr [3], Ge

[21], Al [22], Ti [23], Cd [24], Mn–Zr [25], Cu–Ni [26] and Zn–Zr [27] on various structural, microstructure, electrical, dielectric and magnetic properties has been reported, and a mutual influence between the structure and the cationic distribution is recognized. It seems only very little work has been done so far on the cation distribution of Mg substituted lithium ferrites [28]. Therefore, in the present work, we focused on the synthesis of Mg substituted lithium ferrite using sol–gel auto-combustion method using urea as a fuel. Our previous studied involved that the existence of pure lithium ferrite with good magnetic properties was obtained using urea based on sol–gel reaction method at different calcined temperatures from 400 to 800 °C for 2 h. Hence, the impact of Mg^{2+} ion substitution on the crystal structure, microstructure, conductivity, dielectric and magnetic properties of the new synthesized $Li_{1-x}Mg_{2x}Fe_{5-x}O_8$ nanoparticles with $0.0 \leq x \leq 0.8$ is extensively studied using different physical approaches in this work.

2 Experimental procedure

$Li_{1-x}Mg_{2x}Fe_{5-x}O_8$ with $0.0 \leq x \leq 0.8$ have been synthesized using sol–gel auto-combustion method based on urea as a fuel. Chemically grade ferric nitrate ($Fe(NO_3)_3{\cdot}9H_2O$), lithium nitrate ($LiNO_3{\cdot}3H_2O$), magnesium nitrate ($Mg(NO_3)_2{\cdot}6H_2O$) and urea ($NH_2{\cdot}CO\ NH_2$) were used as starting materials. The aqueous solution of ferric, lithium and magnesium nitrates with Fe^{3+}:Li^{+}:Mg^{2+} molar ratios ($5-x$:$1.5-x$:$2x$) to attain $Li_{1-x}Mg_{2x}Fe_{5-x}O_8$ [1] was gently stirred on hot-plate magnetic stirrer for 15 min. followed with addition of an aqueous solution of urea to the mixtures with continuous stirring. The pH of the solution was adjusted at 7 by adding ammonia solution to form the gel. The solution was evaporated to 80 °C with constant stirring until viscous resin was formed and then dried at 100 °C overnight. For the formation of the Mg substituted lithium ferrite phase, the dry precursors of $Li_{1-x}Mg_{2x}Fe_{5-x}O_8$ with $0.0 \leq x \leq 0.8$ were annealed at the rate of 10 °C/min in static air atmosphere at 800 °C and maintained at the temperature for annealed time 2 h. The measurements were carried out in a current of argon atmosphere. The crystalline phases presented in the different annealed samples were distinguished by X-ray diffraction XRD on a Brucker axis D8 diffractometer using Cu-Kα ($\lambda = 1.5406$ Å) radiation and secondary monochromator in the range 2θ from 20 to 70°. The change in ferrites particles morphologies was adjusted by field emission scanning electron microscope (FE-SEM, QUANTA FEG 250). The ac electrical conductivity for the investigated samples was performed over a temperature range from 30 to 200 °C and frequency range from 20 Hz to 10 MHz using (LCR-8110G) precision LCR meter. The magnetic properties of the ferrites were measured at room temperature using a vibrating sample magnetometer (400-1 VSM, U.S., Lake Shore Co., Ltd., USA) in a maximum applied field of 20 kOe. From the obtained hysteresis loops, the saturation magnetization (M_s), remanence magnetization (M_r) and coercivity (H_c) were determined Fig. 1.

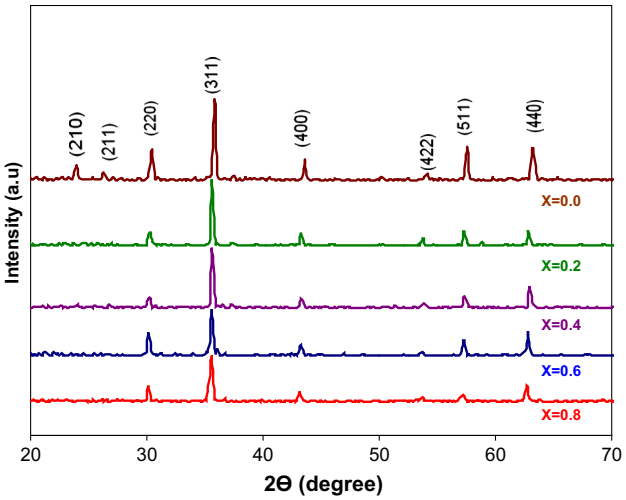

Fig. 1 XRD patterns of $Li_{1-2x}Mg_x\ Fe_5O_8$ with $0.0 \leq x \leq 0.8$ powders annealed at 800 °C for 2 h

3 Results and discussion

3.1 Crystal structure

Figure 2 shows the powder X-ray diffraction patterns of $Li_{1-x}\ Mg_{2x}\ Fe_{5-x}\ O_8$ with $0.0 \leq x \leq 0.8$ powders synthesized by sol–gel auto combustion using urea annealed at 800 °C for 2 h. It was evident that the magnesium substituted lithium ferrite specimens contain single ferrite phase.

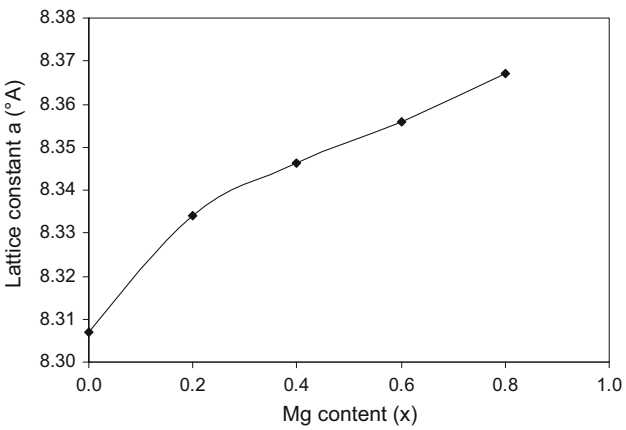

Fig. 2 Dependence of lattice constant versus dopant content of Mg

The diffraction pattern of the unsubstituted sample was exhibited well crystalline cubic $LiFe_5O_8$ (JCPDS # 82-1436) phase. The diffraction peaks belonging to (210) (211) (220) (311) (400) (422) (511) and (400) planes of lithium ferrite were indexed. The introducing of Mg^{2+} ions into pure lithium ferrite phase was executed a small shift towards low 2θ diffraction angle. This shift was slightly increment the lattice parameter. Figure 2 evinces the dependence of the lattice constant on Mg-substituted content. It is clear that the lattice constant was increased with augmenting the magnesium content in the range of $0.0 \leq x \leq 0.8$. It was attributed to the different ionic radii of Fe^{3+} (0.64°A), Mg^{2+} (0.71°A), and Li^{1+} (0.76°A) with a spinel-type structure. The Mg^{2+} ions substituted lithium

Table 1 Average crystallite size, lattice constant and cell volume for $Li_{1-2x}Mg_xFe_5O_8$ ferrite samples annealed at 800 °C for 2 h

x	Average crystallite size (nm)	Lattice constant a (°A)	Cell volume V ($°A^3$)
0.0	91.5	8.307	573.219
0.2	84.8	8.334	578.861
0.4	83.6	8.346	581.398
0.6	75.5	8.356	583.406
0.8	61.5	8.367	585.791

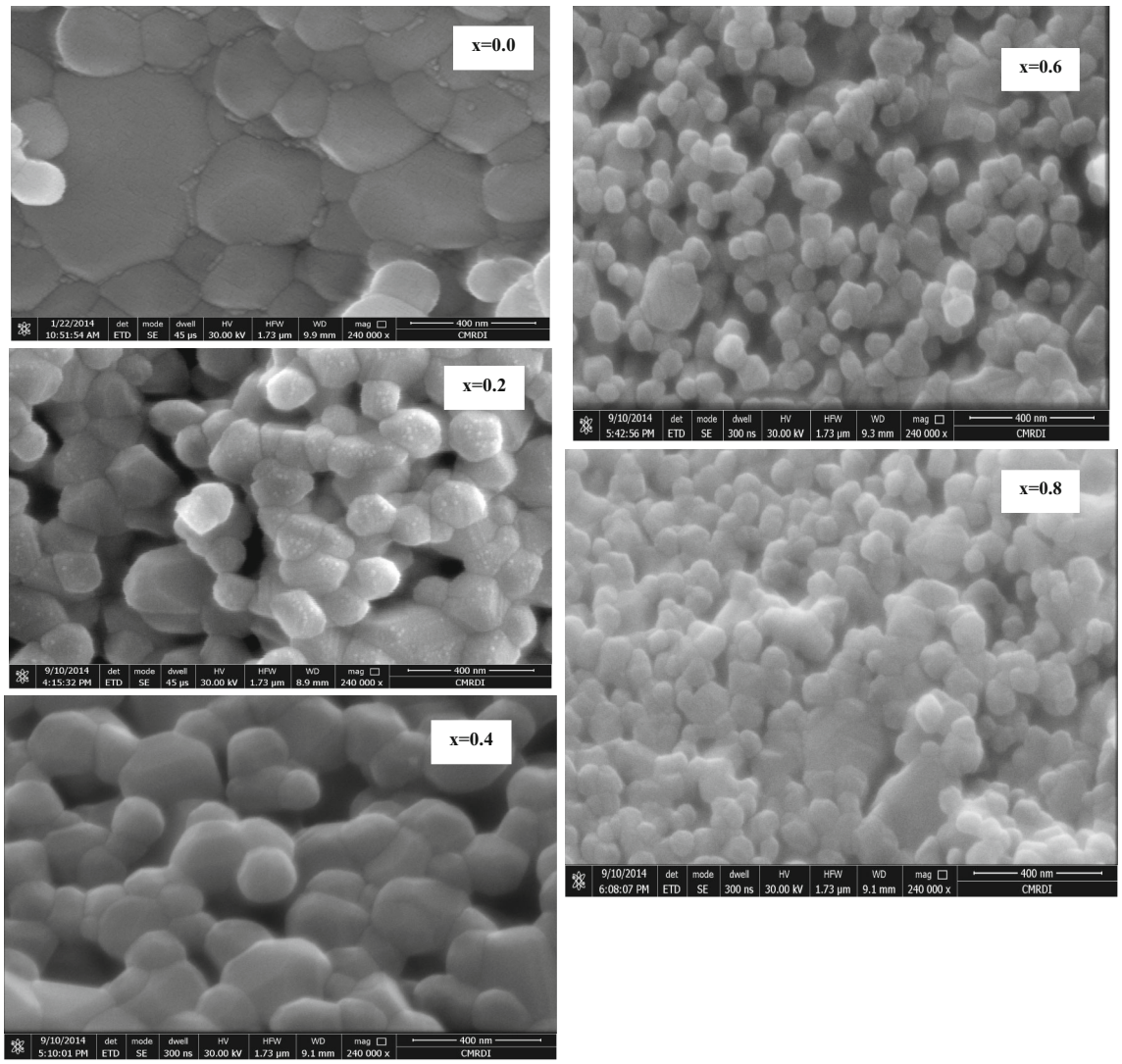

Fig. 3 FE-SEM images of Li1-2xMgxFe5O8 with $0.0 \leq x \leq 0.8$ powders annealed at 800 °C for 2 h

ferrite with larger size compared with Fe^{3+} will induce uniform strain in the lattice as the material is elastically deformed [28]. This effect associated with the lattice plane spacing to change and the diffraction peaks shift to a lower 2θ position. Noticeably, lattice parameter (***a***) as well as unit cell volume (V_{cell}) of the lithium ferrite specimens was calculated and the results were listed in Table 1. The measured lattice parameter for $Li_{1-x}Mg_{2x}Fe_{5-x}O_8$ phase was found to be 0.833 ± 0.01 nm which was in good agreement with that mentioned in the JCPDS card. Alongside, Table 1 also records the crystallite sizes of Li_{1-x} Mg_{2x} Fe_{5-x} O_8 ferrites for the most intense peak [(3 1 1) plane] observed at 2θ ≈ 35.825° based on the XRD data using the Debye–Scherrer formula. It was found that the crystallite size was minified with addition of Mg^{2+} ion. It was found to reduce from 91.5 nm for pure lithium ferrite to 61.5 nm with Mg^{2+} ion substituted molar ratio 0.8.

3.2 Microstructure

Figure 3 displays the field emission scanning electron microscope (FE-SEM) of Li_{1-x} Mg_{2x} $Fe_{5-x}O_8$ with different Mg^{2+} ion content 0.0 ≤ x ≤ 0.8 annealed at 800 °C for 2 h. It is clear that the distribution of the grains with uniform size in each compositions was observed. Besides, the grain size was significantly depended on the Mg-substituted content. The grain size was gradually minimized with

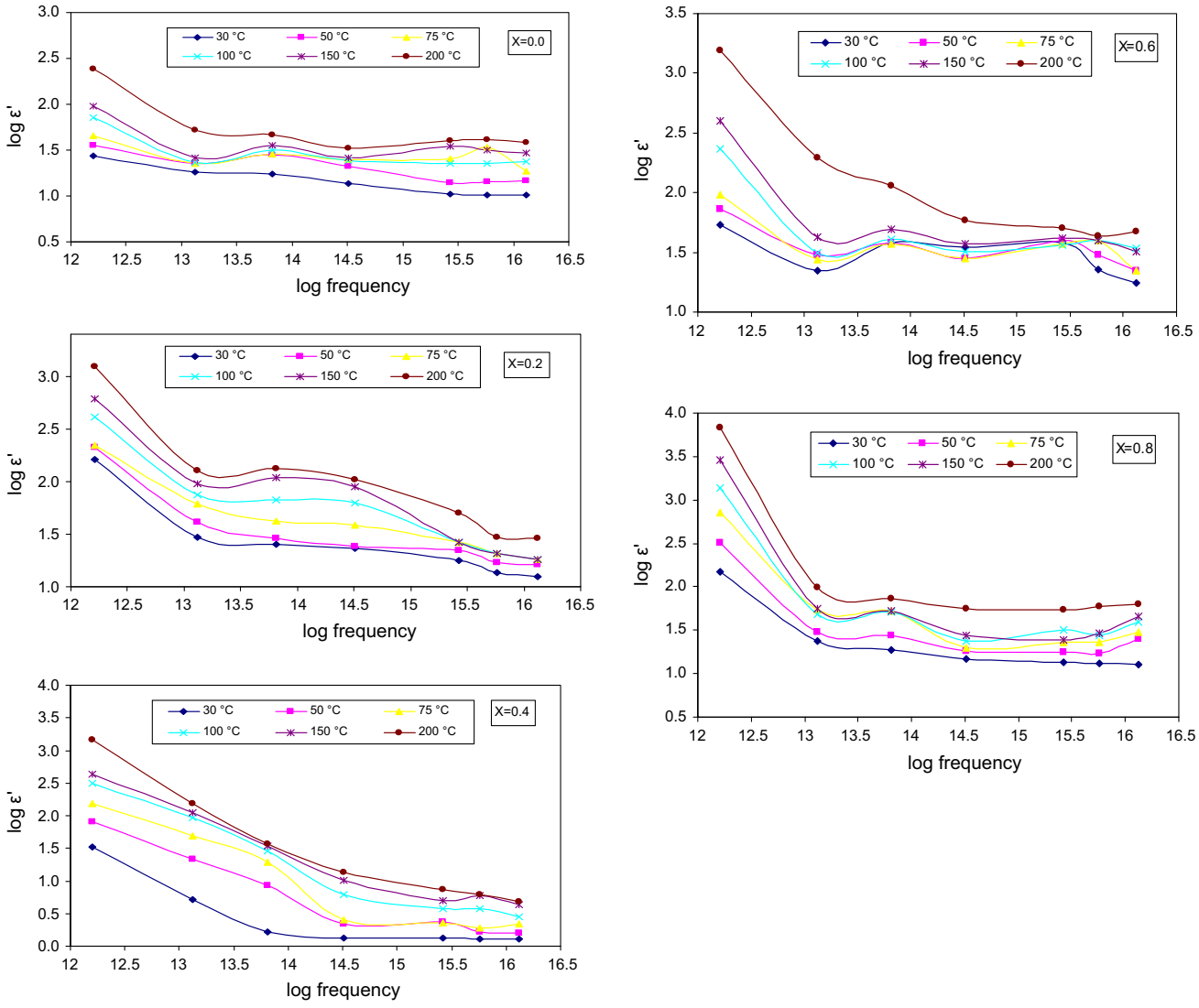

Fig. 4 Frequency dependence of real part of dielectric constant ε′ of $Li_{1-2x}Mg_xFe_5O_8$ with 0.0 ≤ x ≤ 0.8 powders annealed at 800 °C for 2 h

increasing Mg-substituted content. The grain size value was varied from 200 to 500 nm for pure lithium ferrite to ~ 60 nm for lithium ferrite substituted by Mg^{2+} ion molar ratio 0.8. Hence, it can be confirmed that addition Mg^{2+} ion to lithium ferrite was inhibited the grain growth of the formed ferrite. The change in the grain size was attributed to the Mg^{2+} ions (0.71°A) which are substituted Li^{+} ions (0.76°A) occupy tetrahedral site (A) in the spinel lattice with a corresponding migration of Fe^{3+} ions (0.64°A) from A-site to B-site which equilibrates the stress on B-site causing the observed change in the microstructure. Meanwhile, the formed particles was transformed from a quasi-octahedral honey network-like structure to grain patterns exhibited spherical-like structure with increasing the Mg content.

3.3 Dielectric properties

3.3.1 The frequency dependence of dielectric constant (ε′)

Figure 4 indicates the dielectric measurements of the samples over a temperature range from 30 to 200 °C and frequency range from 20 Hz to 10 MHz. The results revealed that the dielectric constant (ε′) was minified with

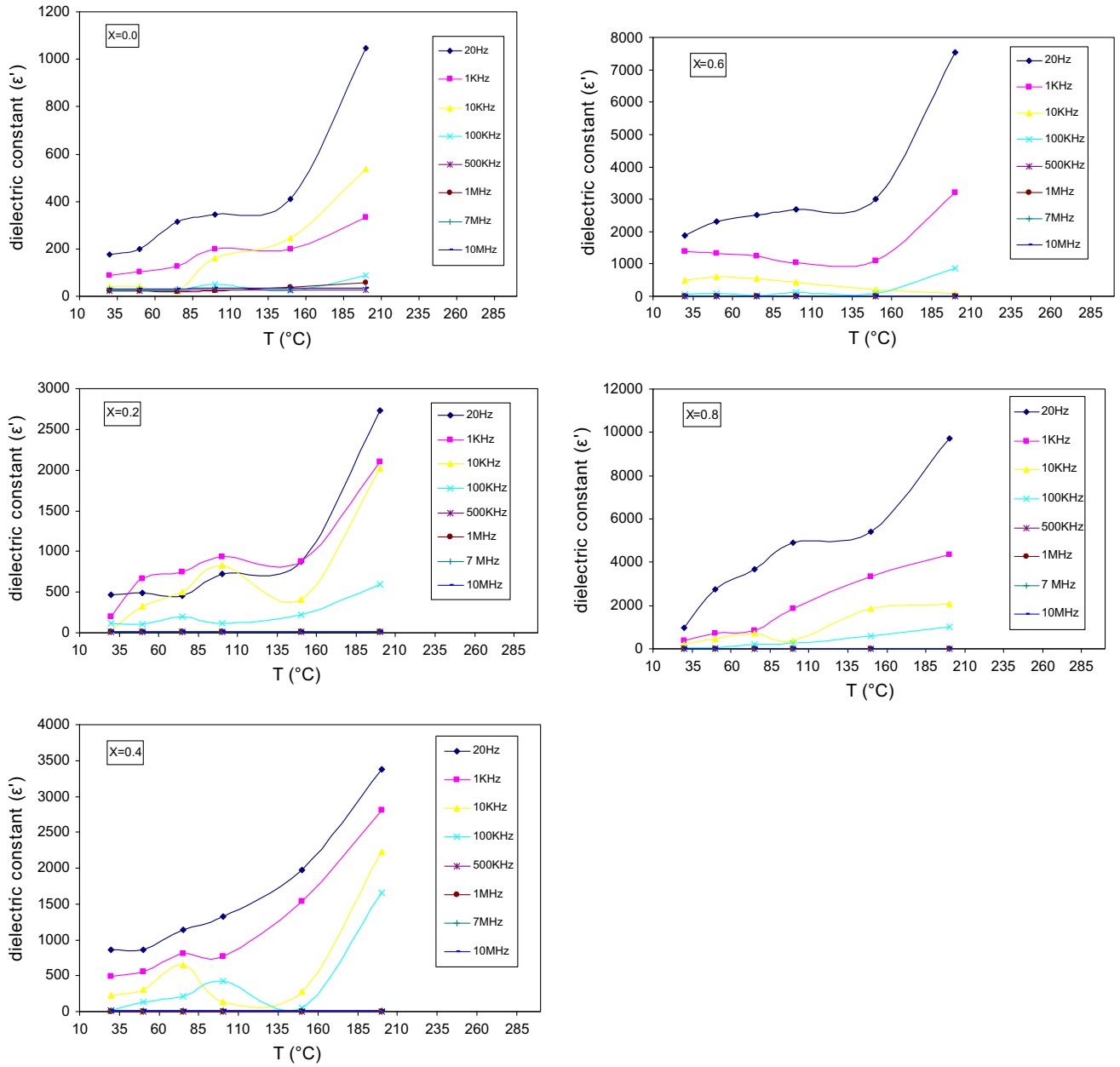

Fig. 5 Temperature dependence of real part of dielectric constant ε′ of $Li_{1-2x}Mg_xFe_5O_8$ with $0.0 \leq x \leq 0.8$ powders annealed at 800 °C for 2 h

enlarging the frequency. All samples were exhibited the similar frequency dependence of ε′. The variation in ε′ with frequency can be understood on the basis of Maxwell and Wagner two layer model in accordance with Koop's phenomenological theory [29]. The dielectric structure of ferrites is made up of well conducting layer of grains followed by poorly conducting layer of grain boundaries and the high value of dielectric constant arises from the space charge polarization produced at the grain boundary. The polarization mechanism involves the exchange of electrons between the ions of the same element, which are present in more than one valence state and are distributed randomly over crystallographic equivalent sites. Here the exchange of electrons mainly takes place between Fe^{3+} and Fe^{2+} ions present at octahedral sites (B-site). During this exchange mechanism, the electrons have to pass through the grains and grain boundary of the dielectric medium. Owing to high resistance of the grain boundary, the electrons accumulate at the grain boundary and produce space charge polarization. Furthermore, it can be seen that the dielectric constant was decreased rapidly in the low frequency region and became frequency independent in the high frequency region. It is well known that the grain boundaries are more effective in low frequency region and the grains are effective in the high frequency region [29]. Therefore, due to the grain boundary effect, the dielectric constant decreases rapidly in the low frequency region. In the high frequency region, the grains come into action and also the hopping of electrons cannot follow the high frequency ac field, therefore, the dielectric constant decreases and becomes frequency independent.

3.3.2 *The temperature dependence of dielectric constant (ε′)*

Figure 5 describes the variation of the dielectric constant ε′ with temperature for all investigated samples of $Li_{1-x}Mg_{2x}Fe_{5-x}O_8$ with $0.0 \leq x \leq 0.8$ powders annealed at 800 °C for 2 h over a temperature range from 30 to 200 °C and frequency range from 20 Hz to 10 MHz. The data showed that dielectric constant ε′ was nearly constant with low temperature and it was slightly changed with the frequency. This behavior can be ascribed to the partially electronic polarization, which played a significant role in this region. Otherwise, a lightly increase in ε′ was observed with raise the temperature. This was attributed to the ionic polarization that beginning to play a role in cooperation with the electronic one. Consequently, the participation of more than one type of polarization led to increasing the value ε′ with temperature. Hence, it can conclude that the dielectric constant is almost temperature independent due to the dipole remained frozen at the relatively low temperature range. Further, more than one type of polarization of the dipoles was expected at relatively high temperature by increasing temperature. Subsequently, the dipoles rotations became easier and thus ε′ was increased with temperature.

3.3.3 *Effect of Mg concentration on dielectric constant (ε′)*

Figure 6 elucidates the effect of Mg concentration (*x*) on dielectric constant at stable temperature 200 °C. It is illuminated that ε′ was increased with increasing the concentration of Mg^{2+} ions. It is known that the Li^+ ions occupy only the octahedral site (B-site) in the spinel lattice whereas the Mg^{2+} ions prefer to occupy both the tetrahedral and octahedral sites [28, 30]. Therefore, with the increase in the concentration of Mg^{2+} ions, some of the Mg^{2+} ions occupy the tetrahedral site (A-site) and so displace the Fe^{3+} ions from A-site to B-site. Thus more Fe^{2+}–Fe^{3+} ion pairs are available at B-site for hopping mechanism which results in the increase in dielectric polarization and hence of the dielectric constant.

3.4 Electrical properties

3.4.1 *The temperature dependence of AC conductivity*

Figure 7 illustrates the temperature dependence of AC conductivity, σ_{ac}, for all investigated samples of $Li_{1-x}Mg_{2x}Fe_{5-x}O_8$ with $0.0 \leq x \leq 0.8$ powders annealed at 800 °C for 2 h over a temperature range from 30 to 200 °C and frequency range from 20 Hz to 10 MHz. The relation between the temperature and AC conductivity σ_{ac} was estimated from the Arrhenius expression as the following:

$$\sigma_{ac} = \sigma_o \exp\left(-E_{a(ac)}/\ kT\right) \quad (1)$$

where σ_o is the pre- exponential factor contains several constants, k is the Boltzmann's constant, T is the absolute

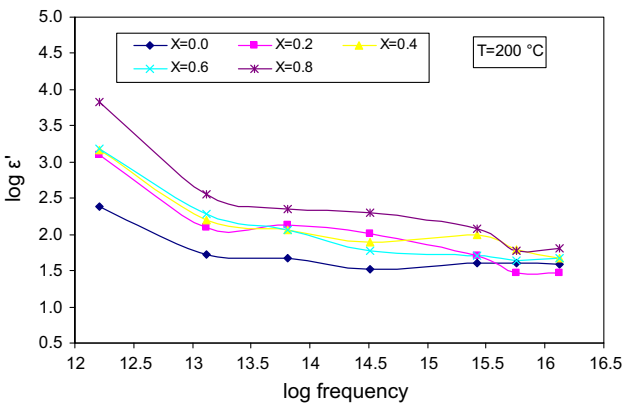

Fig. 6 The dependence of real part of dielectric constant ε′ on Mg content (x) of $Li_{1-2x}Mg_xFe_5O_8$ with $0.0 \leq x \leq 0.8$ powders annealed at 800 °C for 2 h

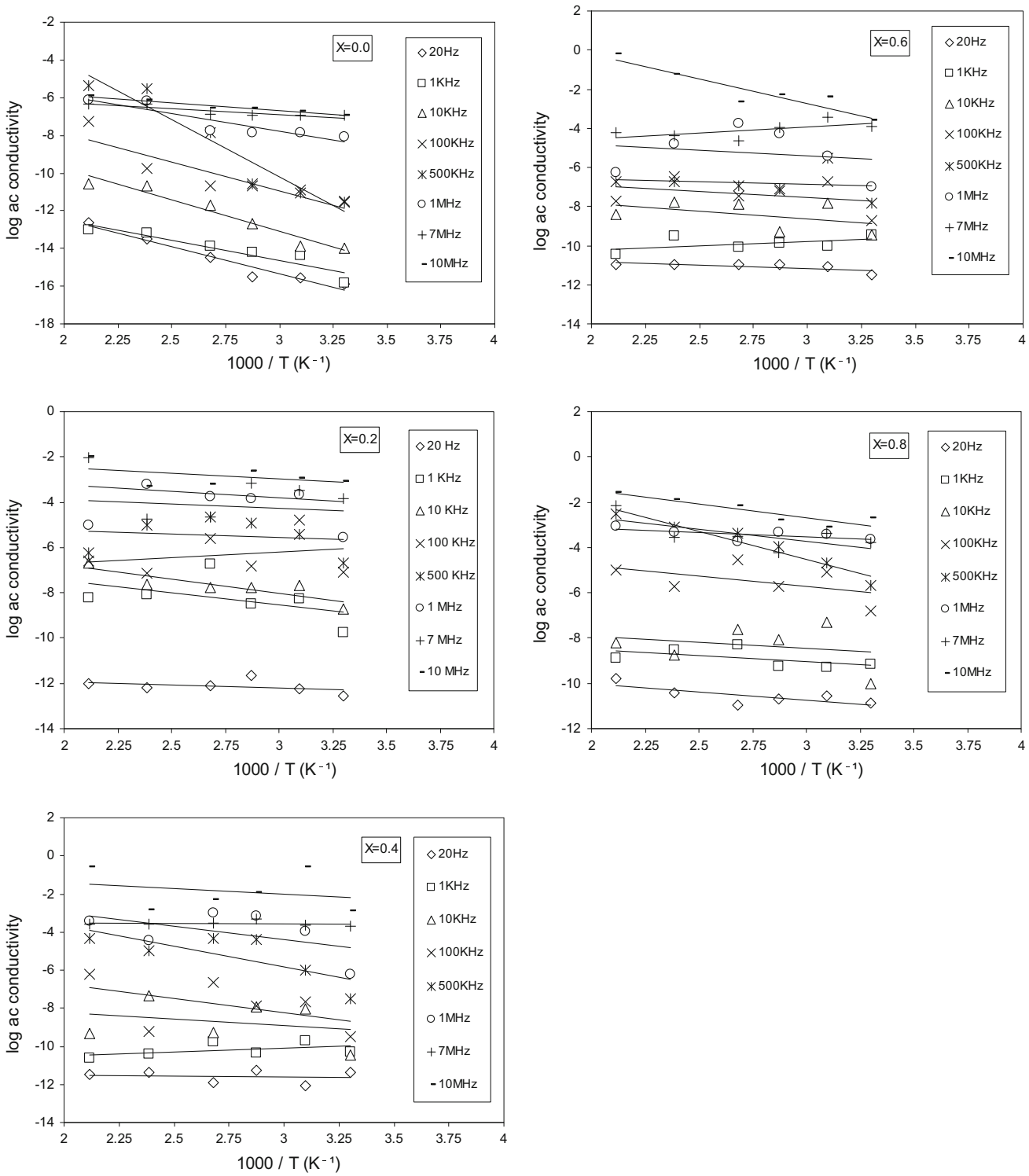

Fig. 7 Electrical conductivity versus inverse of temperatures for $Li_{1-2x}Mg_xFe_5O_8$ with $0.0 \leq x \leq 0.8$ powders annealed at 800 °C for 2 h

temperature and $E_{a(ac)}$ is the AC activation energy for conduction. The activation energies were calculated from straight line fit using Eq. 1 compositions and they were given in Table 2. It is noticeable that the AC conductivity σ_{ac} was steadily increased upon increasing of temperature and Mg2 + ion content. However, the mechanism of electrical conduction is similar to that of dielectric polarization. In the low frequency region, grain boundaries with

Table 2 Activation energies obtained from Arrhenius plots for $Li_{1-2x}Mg_xFe_5O_8$ ferrite samples annealed at 800 °C for 2 h

x	$E_{a(ac)}$ (eV)							
	20 Hz	1 kHz	10 kHz	100 kHz	500 kHz	1 MHz	7 MHz	10 MHz
0.0	0.246	0.183	0.286	0.264	0.521	0.160	0.054	0.073
0.2	0.023	0.092	0.109	0.041	0.028	0.033	0.049	0.041
0.4	0.009	0.036	0.060	0.128	0.188	0.120	0.006	0.049
0.6	0.028	0.039	0.067	0.054	0.022	0.046	0.050	0.215
0.8	0.061	0.045	0.046	0.079	0.215	0.033	0.091	0.104

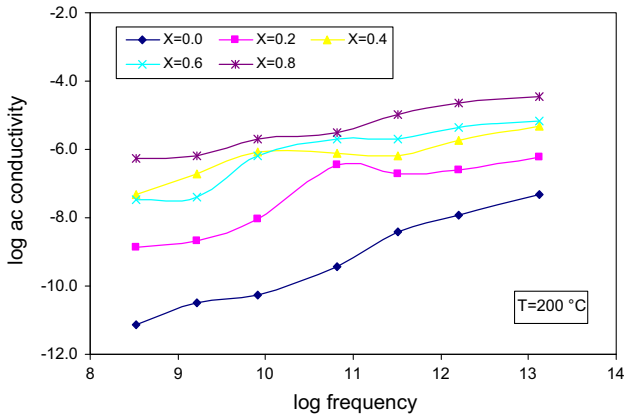

Fig. 8 Dependence of ac electrical conductivity on Mg content (x) of $Li_{1-2x}Mg_xFe_5O_8$ with $0.0 \leq x \leq 0.8$ powders annealed at 800 °C for 2 h

high resistance were effective, giving a constant plateau region (σ_{ac}). At higher frequencies, the increase in conductivity was imputed to grain effect and increased hopping of charge carriers between Fe^{2+}–Fe^{3+} ions at the adjacent octahedral sites [28, 30]. On the other hand, the increase in conductivity with temperature was related to thermally activated hopping of charge carriers [28, 30]. Additionally, the increment of σ_{ac} with Mg^{2+} ions ratio was attributed to the increase in the magnitude of electronic exchange which was dependent on the concentration of Fe^{3+}/Fe^{2+} ion pairs present on B-site as depicted in Fig. 8.

3.4.2 The frequency dependence of AC conductivity

Generally, the total conductivity is expressed bythe following power relation

$$\sigma_{ac}(\omega) = A\,\omega^{s} \quad (2)$$

where A is a temperature dependent parameter, ω is the angular frequency and the frequency exponent s is a temperature-dependent parameter with values between 0.0 and 1. Figure 9 presents the variation of electrical conductivity σ_{ac} (ω) with frequency 20 Hz to 10 MHz. One can note that values of conductivity was gradually increased with increasing the applied field frequency. The increasing in (σ_{ac}) with applied field frequency was explicated in the fact that the pumping force of the applied frequency that helps in transferring the charge carriers between the different localized states as well as liberating the trapped charges from the different trapping centers. These charge carriers participate in the conduction process concurrent with electrons produced from the valence exchange between the different metal ions. The exponent *s* was determined as a function of composition for each samples, in the temperature range from 30 to 200 °C by plotting ln σ versus ln ω according to Eq. 2 as depicted in Fig. 9 which represents straight lines with slope equal to the exponent *s* and the variation of the exponent *s* is given in Table 3. It is obviously that the value of *s* was between 0 and 1. When $s = 0$, the electrical conduction was frequency independent or DC conduction, but for $s \leq 1$, the conduction was frequency dependent or AC conduction. Consequently, it is distinctly that the exponent s was located in two ranges. In the range $0.5 \leq s \leq 1$ which evidenced the electron hopping between Fe^{+2} and Fe^{+3} ions and the values of $s \leq 0.5$ which demonstrated the domination of ionic conductivity [30]. Table 3 devotes the values of s which proved that the exponent s was positioned in the two ranges. Therefore, the manner of σ' with frequency and ***S*** with temperature denoted that the classical barrier hopping model is the most favorable mechanism to expound the conduction mechanism for the compositions under investigation. The charge carriers responsible for the conduction process are the electron hopping between Fe^{2+} and Fe^{3+} ions in the case of Mg-substituted lithium ferrite samples.

3.5 Magnetic properties

The magnetization of Li_{1-x} Mg_{2x} Fe_{5-x} O_8 with $0.0 \leq x \leq 0.8$ powders was measured at room temperature under an applied field of 20 kOe and the hysteresis loops of the ferrite powders were obtained. Figure 10 shows the nexus of magnetization (M) as a function of applied field (*H*). Subsequently, the magnetic parameters are listed in Table 4. It is distinctly that the saturation magnetization of the ferrite powders was increased with increasing the Mg^{2+} content upon $x = 0.4$. Thereafter, it was decreased with

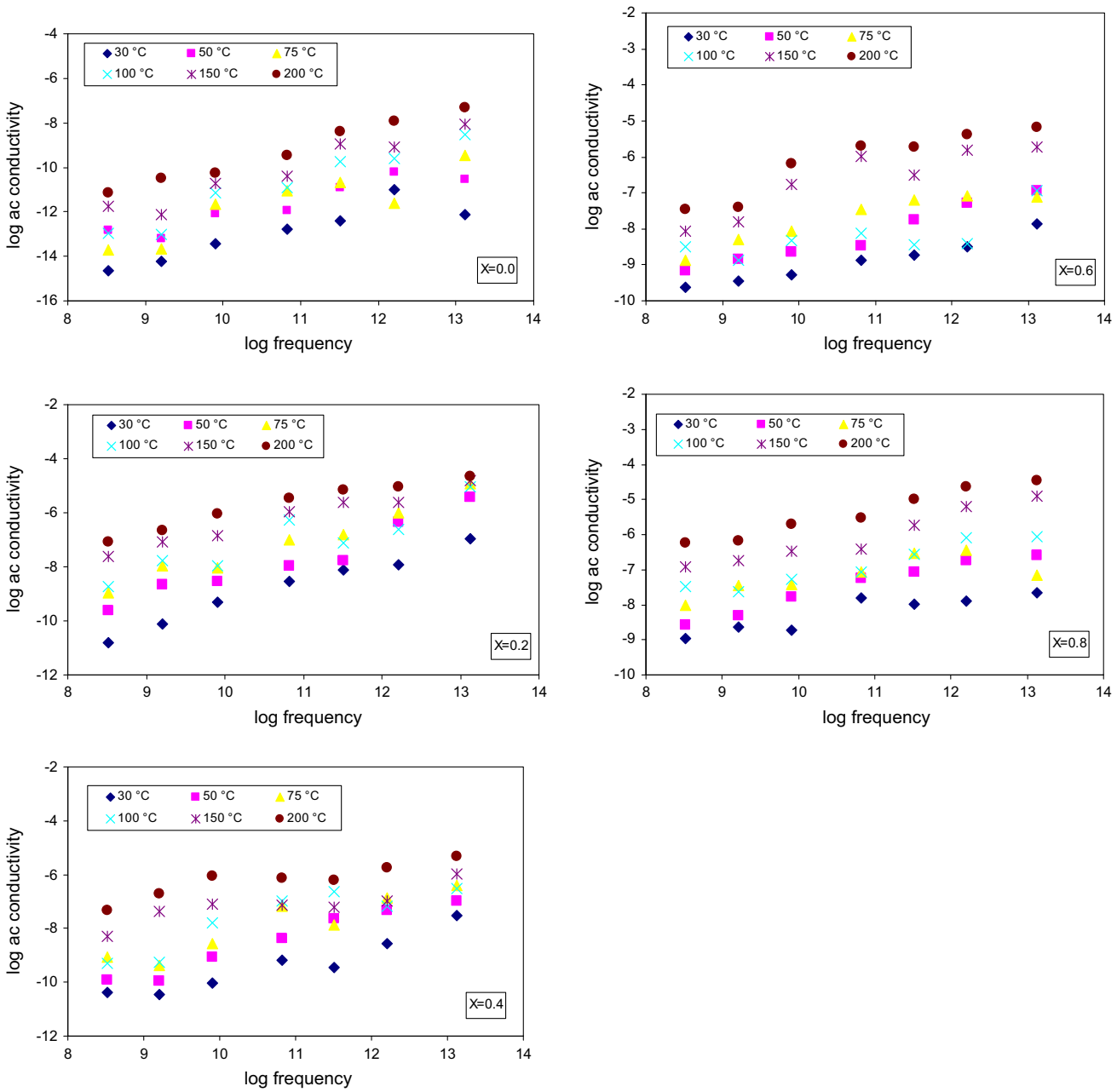

Fig. 9 Dependence of AC conductivity on the frequency of Li_{1-2x} Mg_x Fe_5O_8 with $0.0 \leq x \leq 0.8$ powders annealed at 800 °C for 2 h

$x > 0.4$. The observed magnetization was a result of the simultaneous influence of several extrinsic and intrinsic factors such as density, anisotropy, grain size, cation distribution and the A–B exchange interaction [29–32]. The saturation magnetization is, therefore, explained by considering the metal ion distribution and antiparallel spin alignment of the two sublattice sites. According to Neel's model, of the three types of AA, AB and BB interactions, intersublattice A–B superexchange interaction is the strongest. The net magnetization is given by the vector sum of the magnetization of the two sublattices A and B. The initial increase in *Ms* may be due to the fact that some of the Mg^{2+} ions, which are incorporated in place of Li^{+} ions, occupy tetrahedral site (A) in the spinel lattice with a corresponding migration of Fe^{3+} ions from A-site to B-site. This increases the magnetization of the B sublattice while that of A sublattice decreases as Fe^{3+} ions. With further incorporation of Mg^{2+} ions ($x > 0.4$), the decrease in *Ms* can be attributed to the increased migration of Fe^{3+} ions from the A- to B-site in order to accommodate the Mg^{2+} ions at the A-site. This migration results in an increase in Fe^{3+} ion concentration at B-site which gives rise to

Table 3 The values of the exponent "s value" for $Li_{1-2x}Mg_xFe_5O_8$ ferrite samples annealed at 800 °C for 2 h at different temperatures

x	S-value					
	30 °C	50 °C	75 °C	100 °C	150 °C	200 °C
0.0	0.692	0.648	0.831	0.998	0.874	0.855
0.2	0.798	0.838	0.81	0.673	0.593	0.537
0.4	0.603	0.718	0.645	634	0.351	0.363
0.6	0.362	0.493	0.397	0.262	0.525	0.529
0.8	0.294	0.459	0.252	0.375	0.462	0.427

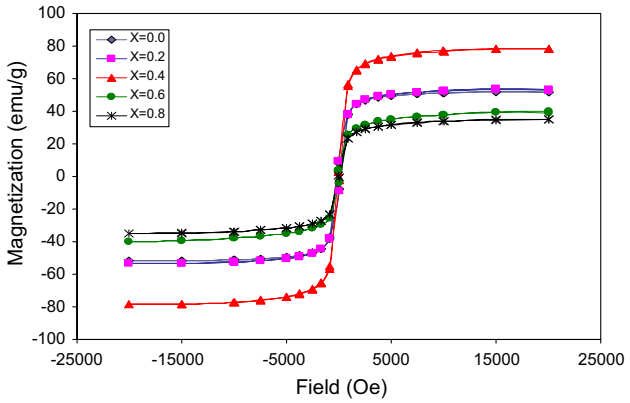

Fig. 10 *M-H* hysteresis loop of $Li_{1-2x}Mg_xFe_5O_8$ with $0.0 \leq x \leq 0.8$ powders annealed at 800 °C for 2 h

Table 4 The magnetic properties for $Li_{1-2x}Mg_xFe_5O_8$ ferrite samples annealed at 800 °C for 2 h

x	*Ms* (emu/g)	*Mr* (emu/g)	*Hc* (Oe)
0.0	51.9	7.96	145.7
0.2	53.6	9.11	162.4
0.4	78.7	2.50	36.0
0.6	34.9	0.62	21.6
0.8	40.3	3.34	97.6

antiparallel spin coupling and spin canting. This results in the weakening of the A–B exchange interaction, leading to the reduction of the magnetization [29–33]. Moreover anomalous behavior of *Hc was* due to the different magnetic moment of Fe and Mg. This may be imputed to changes in the particle size and the low magnetic anisotropy, which arises from crystal imperfection [33, 34].

4 Conclusions

Li_{1-x} Mg_{2x} Fe_{5-x} O_8 with $0.0 \leq x \leq 0.8$ nanopowders have been successfully synthesized by sol–gel auto-combustion method using urea as an organic fuel. The results from XRD, FE-SEM, dielectric constant, AC electrical conductivity and VSM studies are summarized as follows:

- XRD analysis showed that all the samples were formed in single phase cubic spinel structure.
- The introducing of Mg^{2+} ions into pure lithium ferrite phase was occurred a small shift towards low 2θ diffraction angle. Thus, the lattice constant was increased with addition of Mg^{2+} ion.
- The crystallite size of the formed powders was found to minify with increasing the Mg content. It was found to decrease from 91.5 nm for pure lithium ferrite to 61.5 nm with Mg^{2+} ion molar ratio of 0.8.
- The microstructure of Li_{1-x} Mg_{2x} Fe_{5-x} $_{O8}$ with $0.0 \leq x \leq 0.8$ powders was dependent on concentration of magnesium. the formed particles was converted from a quasi-octahedral honey network-like structure to grain patterns exhibited spherical-like structure with increasing the Mg content.
- Dielectric constant (ε') was decreased with the enhancing the frequency of external electric field whereas it was found to increase with temperature.
- Ac conductivity of the formed ferrite powders was slightly increased at low frequencies and abruptly at high frequencies. Moreover, Ac conductivities of these ferrites were increased as the result of the increment of temperature and concentration of Mg^{2+} ions due to increase the hopping of electrons between Fe^{2+} and Fe^{3+} ions.
- The formed crystalline pure magnesium substituted lithium ferrite powders had good magnetic properties. High saturation magnetization (78.7 emu/g) was fulfilled for the formed ferrite at annealing temperature 800 °C for 2 h with Mg content 0.4. Such ferrite nanomaterials would be a good candidate for several potential applications including microwave devices and high-density magnetic recording media. Meanwhile, these ferrite compositions are useful for the multilayer chip inductors which are important components for electronic products such as notebook computer and cellular phone [1, 2].

Acknowledgments This research is financially supported by Science and Technology Development Fund STDF, Egypt, Grant No. Project ID 3681.

References

1. M.M. Rashad, M.G. El-Shaarawy, N.M. Shash, M.H. Maklad, F.A. Afifi, J. Magn. Magn. Mater. **374**, 495 (2015)
2. Dipti, P. Kumar, J.K. Juneja, S. Singh, K.K. Raina, C. Prakash, Ceram. Int. **41**, 3293 (2015)
3. M. Srivastava, S. Layek, J. Singh, A.K. Das, H.C. Verma, A.K. Ojha, N.H. Kim, J.H. Lee, J. Alloys Compd. **591**, 174 (2014)

4. S.A. Mazen, N.A. Abu-Saad, Appl. Nanosci. **5**, 105 (2015)
5. H. Zeng, T. Tao, Y. Wu, W. Qi, C. Kuang, S. Zhou, Y. Chen, RSC Adv. **4**, 23145 (2015)
6. P.V.B. Reddy, B. Ramesh, ChG Reddy, Phys. B **405**, 1852 (2010)
7. A. Sutka, G. Mezinskis, Front. Mater. Sci. **6**, 128 (2012)
8. R.P. Patil, B.V. Jadhav, P.P. Hankare, Results Phys. **3**, 214 (2013)
9. V.S. Sawant, K.Y. Rajpure, J. Magn. Magn. Mater. **382**, 152 (2015)
10. X. Wang, L. Gao, L. Li, H. Zheng, Z. Zhang, W. Yu, Y. Qian, Nanotechnology **16**, 2677 (2005)
11. H. Zeng, T. Tao, Y. Wu, W. Qi, C. Kuang, S. Zhouand, Y. Chen, RSC Adv. **4**, 231–245 (2014)
12. B. Li, Y. Xie, H. Su, Y. Qian, X. Liu, Solid State Ion. **120**, 251 (1999)
13. S. Singhal, K. Chandra, J. Electromagn. Appl. Anal. **2**, 51 (2010)
14. M.A. Dar, J. Shah, W.A. Siddiqui, R.K. Kotnala, J. Alloys Compd. **523**, 36 (2012)
15. M. Rasly, M.M. Rashad, J. Magn. Magn. Mater. **337–338**, 58 (2013)
16. M.M. Rashad, A.O. Turky, A.T. Kandil, J. Mater. Sci.: Mater. Electron. **24**, 3284 (2013)
17. M.M. Rashad, J. Mater. Sci.: Mater. Electron. **23**, 882 (2012)
18. M.M. Rashad, M.G. Fayed, T.M. Sami, E.E. El-Shereafy, J. Mater. Sci.: Mater. Electron. **26**, 1259 (2015)
19. G. Aravind, M. Raghasudha, D. Ravinder, J. Magn. Magn. Mater. **378**, 152 (2015)
20. Viswarupa Mohanty, Rajesh Cheruku, Lakshmi Vijayan, G. Govindaraj, J. Mater. Sci. Technol. **30**, 335 (2014)
21. S.A. Mazen, N.I. Abu-Elsaad, Ceram. Int. **40**, 11229 (2014)
22. P.R. Arjunwadkar, R.R. Patil, J. Alloys Compd. **611**, 273 (2014)
23. B.K. Kuanr, G.P. Srivastava, J. Appl. Phys. **75**, 6115 (1994)
24. T. Namgyal, J. Singh, K. Chandra, S. Bansal, S. Singhal, J. Mol. Struct. **1019**, 103 (2012)
25. M.J. Iqbal, M.I. Haider, Mater. Chem. Phys. **140**, 42 (2013)
26. M. Ramesh, G.S.N. Rao, K. Samatha, B.P. Rao, Ceram. Int. **41**, 1765 (2015)
27. S.K. Gurav, S.E. Shirsath, R.H. Kadam, S.M. Patange, K.S. Lohar, D.R. Mane, Mater. Res. Bull. **48**, 3530 (2013)
28. Y.-P. Fu, S.-H. Hu, Ceram. Int. **36**, 1311 (2010)
29. M.A. Dar, K.M. Batoo, V. Verma, W.A. Siddiqui, R.K. Kotnala, J Alloys Compd. **493**, 553 (2010)
30. A.A. Kadam, S.S. Shinde, S.P. Yadav, P.S. Patil, K.Y. Rajpure, J. Magn. Magn. Mater. **329**, 59 (2013)
31. R. Cheruku, G. Govindaraj, L. Vijayan, Mater. Chem. Phys. **146**, 389 (2014)
32. S.S. Teixeira, M.P.F. Graça, L.C. Costa, M.A. Valente, Mater. Sci. Eng. B **186**, 83 (2014)
33. S.I. Hussein, A.S. Elkady, M.M. Rashad, A.G. Mostafa, R.M. Megahid, J. Magn. Magn. Mater. **379**, 9 (2015)
34. M.M. Rashad, M.I. Nasr, Electron. Mater. Lett. **8**, 325 (2012)